



## ARTICLE

## 4-Methoxydalbergione is a potent inhibitor of human astrogloma U87 cells in vitro and in vivo

Ran Li<sup>1</sup>, Chang-qiong Xu<sup>1</sup>, Jian-xin Shen<sup>1</sup>, Qiu-yun Ren<sup>1</sup>, Di-ling Chen<sup>2</sup>, Mian-jie Lin<sup>1</sup>, Rong-ni Huang<sup>1</sup>, Chun-hui Li<sup>3</sup>, Ru-ting Zhong<sup>1</sup>, Zhi-hua Luo<sup>1</sup>, Xiao-yu Ji<sup>1</sup> and Jie Wu<sup>1</sup>

Astrogloma is the most common primary tumor in the central nervous system without effective treatment strategies. Temozolomide (TMZ) is a chemotherapeutic drug to treat astrogloma but exhibits low potency and has side effects. Therefore, there is an urgent need to develop new compounds to treat astrogloma. *Dalbergia sissou* Roxb was the source of *Dalbergia odorifera* in traditional Chinese medicine (TCM) and has been clinically used as an anti-tumor medicine. 4-Methoxydalbergione (4MOD) is purified from *Dalbergia sissou* Roxb., and shows an inhibitory effect on osteosarcoma, but its effects on astrogloma have not been reported. Here, we evaluate its anti-astrogloma effects on both in vitro and in vivo models. In cultured astrogloma U87 cells, 4MOD inhibited cell proliferation and induced cell apoptosis in a time- and concentration-dependent manner. Compared with TMZ, 4MOD exhibited a tenfold greater potency of anti-astrogloma effects. 4MOD effectively stalled the cell cycle in G2 phase. Transcriptome sequencing (RNA-seq) showed that 4MOD upregulated 158 genes and downregulated 204 genes that are mainly enriched in cell membrane, cell division, cell cycle, p53, TNF, and MAPK signaling pathways, which may underlie its anti-tumor mechanisms. In a nude mouse xenograft model transplanted with U87 cells, 10 mg/kg 4MOD slowed down tumor growth rate, while at 30 mg/kg dose, it reduced tumor size. Collectively, this study demonstrates that 4MOD is a potent native compound that remarkably inhibits U87 astrogloma growth in both in vitro and in vivo models.

**Keywords:** *Dalbergia sissou* Roxb; 4-methoxydalbergione; human astrogloma U87 cell line; RNA-seq; cell cycle; apoptosis

*Acta Pharmacologica Sinica* (2021) 42:1507–1515; <https://doi.org/10.1038/s41401-020-00560-w>

## INTRODUCTION

Cancer has become a leading cause of death globally in the twenty-first century [1]. Glioblastoma is the most common primary brain tumor, and the astrocytomas account for about 65% of brain glioblastomas. These tumors are characterized by aggressiveness and a short overall survival rate [2]. Astrogloma is rarely cured, and its poor prognosis is largely attributed to the proliferative and invasive nature of the disease. Treatment of malignant astrogloma mainly includes surgery, radiotherapy and chemotherapy, with chemotherapy being the standard care. The addition of TMZ to radiotherapy can improve patient survival [3]. TMZ is the first-line drug for astrogloma treatment, but its low potency, serious side effects, and induced astrogloma cell resistance [4] are major disadvantages. Therefore, new compounds to treat astrogloma are needed.

*Dalbergia odorifera* has the effects of promoting qi, blood activating and stasis eliminating, analgesia and hemostasis in TCM [5]. The heartwood of *Dalbergia sissou* Roxb was the source of *D. odorifera* in TCM. *D. odorifera* has been used clinically as a common anti-tumor medicine. However, there is not enough scientific evidence to fully support its medicinal properties since the active ingredients are not well known. In our previous studies, seven flavonoids were isolated and purified from *D. sissou* Roxb. Their chemical structures were elucidated by nuclear magnetic

resonance (NMR) and mass spectrum (MS). In this study, we focus on 4MOD, a flavonoid-containing methoxy groups, flavonoids-containing methoxy groups have shown selective cytotoxicity toward cancer cells, but not to normal cells [6]. Recent research has reported that 4MOD possesses pharmacological effects of anti-osteosarcoma [7]. In addition, 4MOD showed anti-inflammatory and cytoprotective effects on hippocampal BV2 microglia cells in mice and primary microglia in rats [8]. It has also shown antihistamine activity [9].

Therefore, this study aimed to investigate the pharmacological effects of 4MOD on U87 astrogloma cells in vitro and in vivo. Our results demonstrate that 4MOD increases U87 cell apoptosis and cell cycle arrest, and inhibits tumor cell growth in both in vivo and in vitro models. These results suggest that 4MOD is a novel, promising compound that can be developed to treat glioblastoma.

## MATERIALS AND METHODS

## Preparation of 4MOD

4MOD (98% purity, MW = 254.28) was isolated and purified from ethanolic extract of *D. sissou* Roxb. It is a yellow needle-like crystal. EI-MS *m/z*, molecular ion peak 255.1[M + H]<sup>+</sup>; NMR data attribution: <sup>1</sup>H NMR (CDCl<sub>3</sub>, 500 MHz) δ:5.92 (1H, s, H-3), 6.49 (1H, d,

<sup>1</sup>Brain Function and Disease Laboratory, Shantou University Medical College, Shantou 515041, China; <sup>2</sup>Guangdong Institute of Microbiology, Guangzhou 510070, China and

<sup>3</sup>Yueyang Hospital of Traditional Chinese Medicine, Yueyang 414000, China

Correspondence: Xiao-yu Ji (xiaoyu3463@outlook.com) or Jie Wu (jiwu@stu.edu.cn)

Received: 15 May 2020 Accepted: 19 October 2020

Published online: 11 December 2020

$J = 1.2$  Hz, H-6), 4.93 (1H, br.d,  $J = 6.7$  Hz, H-7), 6.10 (1H, ddd,  $J = 17.2, 10.3, 6.7$  Hz, H-8), 5.00 (1H, dt,  $J = 17.2, 1.3$  Hz, H-9a), 5.28 (1H, dt,  $J = 10.3, 1.3$  Hz, H-9b), 7.19 (2H, br.d,  $J = 7.4$  Hz, H-2', H-6'), 7.32 (2H, br. t,  $J = 7.4$  Hz, H-3', H-5'), 7.24 (1H, br.t,  $J = 7.4$  Hz, H-4'), 3.81 (3H, s, 4-OCH<sub>3</sub>). <sup>13</sup>C NMR(CDCl<sub>3</sub>, 125 MHz)  $\delta$ :151.0 (C-1), 186.3 (C-2), 107.9 (C-3), 158.4 (C-4), 182.4(C-5), 131.6 (C-6), 47.0 (C-7), 137.2 (C-8), 118.2 (C-9), 139.3 (C-1'), 128.5 (C-2', C-6'), 128.7 (C-3', C-5'), 127.2 (C-4'), 56.3 (4-OCH<sub>3</sub>) [10]. In cell experiments, the solvent was 0.3% DMSO and 0.05% Tween 20. In animal experiments, the solvent was 0.25% EtOH and 0.25% Cremophor EL.

#### Cell culture

U87 astrogloma cells (ATCC version, were obtained from professor Yi Guan of the Joint Institute of Virology Shantou University- The University of Hong Kong), U251 astrogloma cells (Suzhou Institute of Cell Biology, Chinese Academy of Sciences), and BV2 microglia cells (Guangdong Institute of Microbiology) were cultured in DMEM (Gibco, USA) supplemented with 10% FBS (Gibco, USA), penicillin (100 U/mL) and streptomycin (100  $\mu$ g/mL) at 37 °C in a humidified atmosphere of 5% CO<sub>2</sub>.

#### Cell cytotoxicity and proliferation assays

Cell proliferation was determined by using a Cell Counting Kit-8 (CCK-8, Meilunbio, Dalian, China) assay to detect NADH-dependent dehydrogenase activity as described below. Cells were seeded into a 96-well plate ( $2 \times 10^3$  cells/well) with 100  $\mu$ L of culture medium. After a 12 h incubation, the cells were treated with various concentrations of 4MOD (0, 2.5, 5.0, 10.0, 25.0, 50.0, and 100.0  $\mu$ M) for 24, 48, and 72 h. TMZ (0–200.0  $\mu$ M, Meilunbio, Dalian, China) was used as a positive control. Next, 10  $\mu$ L CCK-8 solution was added to each well and cells were incubated at 37 °C for 2 h. Absorbance was measured at 450 nm using a microplate reader (Bio Tek Elx800, USA).

The inhibition and the median inhibitory concentration (IC<sub>50</sub>) were calculated from the cytotoxicity curves. Inhibition was calculated by the following formula: Inhibition = (Ac – As)/(Ac – Ab)  $\times$  100% (Ac, As, and Ab are the absorbance of control well, sample well and blank well, respectively). Drug concentrations and cell inhibition were used to plot a dose–response curve. IC<sub>50</sub> was calculated from concentration vs. percent inhibition curves. Cell morphological changes were observed using an inverted microscope (Zeiss, Axio Observer A1, Oberkochen, Germany).

#### Annexin V-FITC/PI cell apoptosis analysis

Cell apoptosis was analyzed with an Annexin V-FITC/PI apoptosis detection kit (Absin Bioscience Inc, Shanghai, China). U87 cells were seeded in a six-well plate ( $1 \times 10^6$  cells/well) and incubated at 37 °C for 48 h in medium (treated with 4MOD, 0–10.0  $\mu$ M; positive control was TMZ, 0–100.0  $\mu$ M). The cells were collected and washed twice with ice-cold PBS and stained with Annexin V-FITC for 15 min. PI staining was performed 5 min before evaluation by flow cytometry (BD Accuri™ C6, BD Biosciences, San Jose, CA). Data analysis was performed with BD Accuri C6 software (Version 1.0.264.21).

#### Cell cycle analysis

Cell cycle analysis was performed using a Cell Cycle Staining Kit (Abbkine, Wuhan, China). U87 cells were seeded in a six-well plate ( $1 \times 10^6$  cells/well) and incubated for 4 h. Cells were first synchronized by serum starvation, then drug-containing medium (4MOD, 0–10.0  $\mu$ M; positive control was TMZ, 0–100.0  $\mu$ M) was added for 48 h. The cells were collected and fixed with chilled 70% ethanol for 24 h at 4 °C. Next, the fixed cells were washed with ice-cold PBS and stained with PI at 37 °C for 30 min in the dark, then fluorescence was detected by flow cytometry (Ex/Em = 535/615 nm, BD Accuri™ C6, BD Biosciences, San Jose, CA). Cell cycle distribution was determined using FlowJo cell cycle analysis software (Version 7.61, Version V10.5).

Total RNA isolation and transcriptome sequencing  
U87 cells were seeded in a six-well plate ( $1 \times 10^6$  cells/well) and incubated for 12 h, then treated with 4MOD (0  $\mu$ M and 5.0  $\mu$ M for 12 h). Total RNA was isolated using an RNAeasy™ RNA extraction kit (Beyotime, Shanghai, China), after which RNA purity and concentration were determined using a Nanodrop 2000 spectrophotometer (Implen, Los Angeles, USA). After total RNA was extracted and mRNA was enriched by using oligo(dT) beads and a Ribo-Zero™ Magnetic Kit (Epicentre, Madison, WI, USA). The enriched mRNA was fragmented into short fragments using fragmentation buffer and reverse transcribed into cDNA with random primers. Second-strand cDNA was synthesized by DNA polymerase I, RNase H, dNTP, and buffer. Then the cDNA fragments were purified with a QIAquick PCR extraction kit, end-repaired, poly(A) tailed, and ligated to Illumina sequencing adapters. The ligation products were size selected by agarose gel electrophoresis, PCR amplified, and sequenced using an Illumina HiSeq™ 2500 platform by Gene Denovo Biotechnology Co. (Guangzhou, China).

#### qRT-PCR analysis

Based on the RNA-seq results, relevant genes were selected, and primers were designed using Primer Premier 5 software (Primer sequences are shown in Table 1). Reverse transcription into cDNA was performed using a cDNA Synthesis SuperMix for qPCR Kit (Transgen, Beijing, China) and the cDNA was amplified using an RT-PCR amplification kit (PerfectStart Green qPCR SuperMix) (Transgen, Beijing, China). The 2<sup>– $\Delta\Delta$ Ct</sup> method was used to perform analysis with GAPDH as the reference gene.

#### Examination of the ability of 4MOD to cross the blood–brain barrier (BBB)

Ten-week-old C57BL/6J mice ( $n = 3$ ) were injected (i.p.) with 4MOD (10 mg/kg in NS, 1.0% EtOH and 1.0% Cremophor EL). After 5, 25, 40, 60, and 120 min, brain tissue homogenate was extracted after anesthesia and normal saline irrigation. After centrifugation (5 min at 14,000 r/min, 4 °C), the supernatant was taken out and precipitated into 1 mL methanol for ultrasonic extraction, centrifuged again. The supernatant was combined and freeze dried, and the product was redissolved with methanol (250  $\mu$ L), and filtered through a 0.22  $\mu$ m pore size filter prior to detection. Chromatographic separation of compounds from brain tissue was conducted using an LCMS-2020 (Shimadzu, Japan) fitted with a Waters Symmetry C<sub>18</sub> column (3.5  $\mu$ m, 100 mm  $\times$  3.0 mm i.d.). Mobile phase gradient as follows: mobile phase A, 60% at 0 min, 70% at 5 min, 100% at 10 min, and 60% at 15 min. The flow rate was 300  $\mu$ L/min and temperature was 40 °C. SPD20A UV diode array detector was monitored at 280 nm.

#### In vivo assessment of the anti-tumor effect of 4MOD in BALB/c-nu mice

Thirty-four 6-week-old male BALB/c nude mice were purchased from Huafukang (Beijing, China). Briefly, U87 cells ( $2 \times 10^6$  cells/0.1 mL PBS/mice) were injected subcutaneously into the right-lower flanks. After 20 days, mice were injected (i.p.) with 4MOD (0, 10, and 30 mg/kg in NS, 0.25% EtOH and 0.25% Cremophor EL) and TMZ (30 mg/kg) once per 3 days for 4 weeks. Tumor size was determined every 3 days using a 3D imaging platform (Vevo® 2100 small animal ultrasonic imaging platform, FUJIFILM Visual-Sonics, Canada). VsiApp (version-3.0.0) was used to determine the areas of cross-sections every 1.0 mm, which were 3D fitted to form a 3D image of the tumor, and the tumor volume was automatically calculated. At the end of the experiment, the tumors were stripped and weighed.

Hematoxylin-eosin(H&E) staining for liver and kidney tissue  
In order to explore the toxicity of 4MOD, we verified the liver and kidney tissues side effect in mice models. Liver and kidney tissues

**Table 1.** QPCR primer sequences.

Gene	Primer sequence	Annealing T (°C)
GAPDH	5'-GTCTCTCTGACTTCAACAGCG-3'	59.5
	5'-ACCACCTGTTGCTGTAGCCAA-3'	59.5
BCL-2	5'-TGTGGATGACTGAGTACCTGAAC-3'	57.8
	5'-AGACAGCCAGGAGAAATCAA-3'	53.7
IL-6	5'-AGACAGCCACTCACCTCTTCAG-3'	59.5
	5'-TTCTGCCAGTGCCTCTTTGCTG-3'	59.5
ATF4	5'-TCAAACCTCATGGGTTCTCC-3'	55.4
	5'-GTGTCATCCAACGTGGTCAG-3'	57.4
SESN2	5'-AGATGGAGAGCCGCTTTGAGCT-3'	59.5
	5'-CCGAGTGAAGTCTCATATCCG-3'	59.5
CCNB1	5'-TGTTGGTTTCTGCTGGGTG-3'	55.4
	5'-TGCCATGTTGATCTTCGCT-3'	55.4
HSPB1	5'-CTGACGGTCAAGACCAAGGATG-3'	59.5
	5'-GTGTATTCCGCGTGAAGCACC-3'	59.5
IL-1A	5'-TGTATGTGACTGCCAAGATGAAG-3'	57.9
	5'-AGAGGAGGTTGGTCTCACTACC-3'	59.5
CCNA2	5'-CAACCAGAGCAGCACAAAGTAGC-3'	59.6
	5'-CTGTGGTCTTTGAGGTAGGTC-3'	59.5
CCNB2	5'-CAACCAGAGCAGCACAAAGTAGC-3'	59.5
	5'-GGAGCCAACCTTTCCATCTGTAC-3'	59.8
CDC20	5'-CGGAAGACCTGCCGTTACATTC-3'	59.5
	5'-CAGAGCTTGCACTCCACAGGTA-3'	59.5
MCM7	5'-GCCAAGTCTCAGCTCCTGTCAT-3'	59.5
	5'-CCTCTAAGGTCAGTTCTCCACTC-3'	59.6
PLK1	5'-GCACAGTGTCAATGCCTCCAAG-3'	59.5
	5'-GCCGTAAGTGTCCGAATAGTCC-3'	59.5
BUB1B	5'-GTGGAAGAGACTGCACAACAGC-3'	59.5
	5'-TCAGACGCTTGCTGATGGCTCT-3'	59.5
BUB1	5'-GCTCTGTCAGCAGACTTCTTC-3'	59.5
	5'-CAGCAGATGTGAAGTCTCCTGG-3'	59.5
CDK1	5'-GGAAACCAGGAAGCCTAGCATC-3'	59.5
	5'-GGATGATTCAGTGCCATTTGCC-3'	57.8
MAP2K6	5'-GGCTACTTGGTGGACTCTGTTG-3'	59.5
	5'-CATCGTGATGCCAGACTCCAA-3'	59.5
RRM2	5'-CTGGCTCAAGAAACGAGGACTG-3'	59.5
	5'-CTCTCTCCGATGGTTGTGTAC-3'	59.6
p53	5'-TGGATGGTGTACAGTCAGAGC-3'	59.5
	5'-TGGATGGTGTACAGTCAGAGC-3'	59.5
BAX	5'-TCAGGATGCGTCCACCAAGAAG-3'	59.5
	5'-TGTGTCCACGGCGCAATCATC-3'	59.6

were harvested for pathological analysis after 4MOD treatment (dose: 30 mg/kg). The morphology of liver and kidney tissues was observed by H&E staining to evaluate the hepatorenal toxicity of 4MOD. Liver and kidney tissues were embedded in paraffin, sectioned (4 µm), stained with H&E, dehydrated, cleared and sealed with neutral gum before microscopic inspection (Nikon Eclipse CI).

#### Statistical analysis

Data were analyzed using Graph Pad Prism software (version 5). Data are presented as the mean ± SEM. Statistical analysis of multiple group comparisons was performed by two-way ANOVA (CCK8 analysis, IC<sub>50</sub>, apoptotic rate, cell cycle, q-PCR and tumor volume) and one-way ANOVA (tumor weight). Significance was

defined at \**P* < 0.05, \*\**P* < 0.01, \*\*\**P* < 0.001, and \*\*\*\**P* < 0.0001 vs. the control group.

## RESULTS

### 4MOD can cross BBB

Previous studies have reported that 4MOD accounts for 0.047%–1.240% in the heartwood of *D. sissoo* Roxb [11]. NMR and MS were used to confirm the chemical structure. UPLC analysis showed that the purity was more than 98% (Fig. S2a). The retention time of 4MOD peak was 6.9 min (Fig. S2a). Brain sample with 4MOD injection was consistent with it (Fig. S2c). There was no response peak in the brain tissue of solvent group (Fig. S2b). These results indicate that 4MOD can penetrate BBB and reach a peak concentration at 40 min after administration (Fig. S2f).

### 4MOD affects cell morphology and suppresses cell proliferation of U87 astrogloma

To evaluate pharmacological effects of 4MOD, we used human U87 cells (cultured from a grade III astrocytoma-glioblastoma of a 44-year-old woman). U87 cells were treated with different concentrations of 4MOD for 24, 48, and 72 h, then examined for cell morphological changes. At 2.5 µM 4MOD, the treated cells exhibited morphological changes, such as cell rounding and the disappearance of protruding spike. At the relatively high dose of 5.0 µM 4MOD, treated cells showed cell shrinking, disappearance of spikes, and detachment from the substrate compared with untreated cells. However, the TMZ (a positive control) indicated that similar morphological changes needed 50 µM (Fig. 1a). Determination of cell viability, using a CCK-8 assay, showed that 4MOD treatment remarkably inhibited U87 cell growth in a concentration-dependent manner. The IC<sub>50</sub> values of 4MOD-induced inhibition at 24, 48, and 72 h were 12.05 ± 1.98, 4.30 ± 0.74, and 5.00 ± 0.83 µM, respectively (Fig. 1b). IC<sub>50</sub> values of TMZ at 24 h, 48 h, and 72 h were 89.12 ± 9.87, 78.03 ± 13.76, and 58.00 ± 7.32 µM, respectively (Fig. 1c). In comparing IC<sub>50</sub> values between 4MOD and TMZ, 4MOD exhibited tenfold higher potency of inhibition for U87 cell growth (Fig. 1d, *P* < 0.01, and *P* < 0.001 vs. the TMZ group).

### 4MOD affects cell morphology and suppresses cell proliferation of U251 astrogloma

Then, we evaluated and compared the effects of 4MOD and TMZ on another astrogloma tumor cell line (U251). The results showed that in the 4MOD-treated group (above 5.0 µM), cells exhibited morphological changes that included cells shrinking, disappearance of spiked protrusions and detachment from the substrate compared with the untreated control cells, while TMZ showed similar effect on cell morphological changes required 50 µM and above (Fig. S3a). Further, 4MOD treatment inhibited U251 cell growth between 2.5 and 100 µM (Fig. S3b), while TMZ inhibited U251 cell growth between 5.0 and 200 µM (Fig. S3c). Statistical analyses showed that the IC<sub>50</sub> values for 4MOD at 24, 48, and 72 h were 18.3 ± 7.32, 14.6 ± 0.88, and 13.3 ± 1.22 µM, respectively (Fig. S3b), whereas those for TMZ at 24, 48, and 72 h were 99.33 ± 9.88, 77.13 ± 2.24, and 62.44 ± 6.29 µM, respectively (Fig. S3c). In four tested cases, comparison between 4MOD and TMZ, the differences of IC<sub>50</sub> values were highly significant at 24 (*P* < 0.0001), 48 (*P* < 0.0001), and 72 h (*P* < 0.001) treatments, respectively (Fig. S3d).

### 4MOD induces cell apoptosis and cell cycle arrest

To evaluate the effects of 4MOD on cell apoptosis, U87 cells were treated with different concentrations of 4MOD and TMZ, then examined for cell apoptosis by Annexin V-FITC/PI flow cytometry (Fig. 2a). After treated with 2.5, 5.0, and 10.0 µM 4MOD, the early apoptotic rate increased from 8.91% ± 1.22% (untreated control group) to 22.41% ± 3.91%, and 26.88% ±

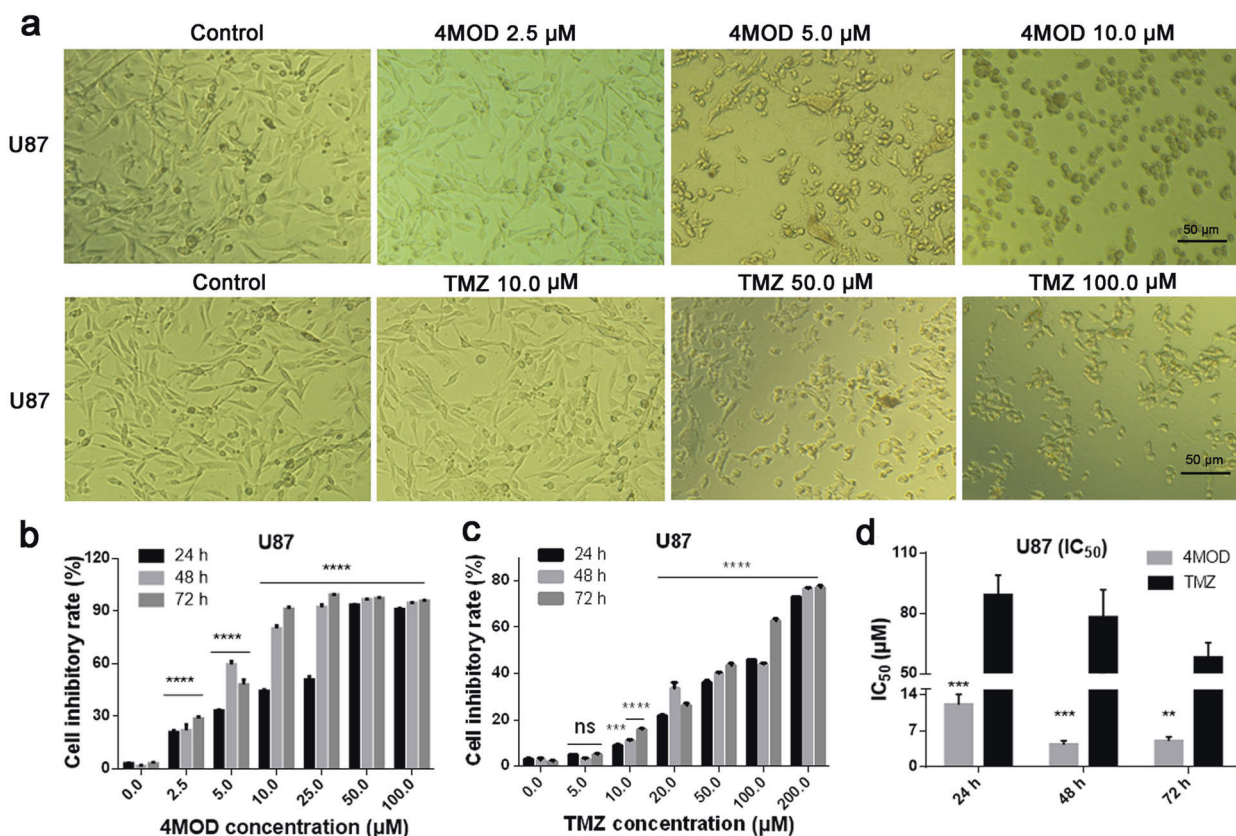


**Fig. 1** Effects of 4MOD and TMZ on cell growth of U87 astrogloma cells. **a** Morphological and cell density changes of U87 cells observed after 48 h treatment with different concentrations of 4MOD (top) and TMZ (bottom). **b** Effects of 4MOD on U87 cell proliferation using a CCK-8 assay. Bar graph shows that 4MOD inhibited U87 cell proliferation in a concentration-dependent manner between 2.5 and 25.0 μM, but did not show a treatment time-dependent manner between 48 and 72 h. **c** Effect of TMZ on U87 cell proliferation. TMZ inhibited U87 cell proliferation, like 4MOD, but with lower potency. **d** IC<sub>50</sub> after 4MOD and TMZ treatment in U87 cells at different treatment time. Data are presented as the mean ± SEM, *n* = 5, \*\*\**P* < 0.001, \*\*\*\**P* < 0.0001 vs. control group for (b) and (c), and in (d), \*\**P* < 0.01 and \*\*\**P* < 0.001 present the comparisons between 4MOD and TMZ.

3.42%, then decreased to 9.12% ± 5.43%, respectively. The decrease of early apoptosis at 10.0 μM 4MOD may be due to the rapid occurrence of late apoptosis and even death of tumor cells. Late apoptotic rate increased from 1.02% ± 0.11% (control) to 2.52% ± 1.45%, 12.59% ± 1.48%, and 52.19% ± 9.32% at 2.5, 5.0, and 10.0 μM 4MOD, respectively. Thus, the total apoptotic rate increased from 9.78% ± 1.04% (control) to 24.33% ± 2.87%, 39.37% ± 4.19%, and 60.99% ± 7.98% at 2.5, 5.0, and 10.0 μM 4MOD, respectively (Fig. 2b). There was a significant difference between early and total apoptosis at 2.5 μM (*P* < 0.01 vs. control). The apoptosis rates of TMZ group were 12.90% ± 1.87%, 32.04% ± 4.93%, and 47.03% ± 4.49% at 10.0 (*P* > 0.05 vs. control), 50.0 (*P* < 0.01 vs. control), and 100.0 μM (*P* < 0.0001 vs. control), respectively (Fig. 2c). There was the significant differences between late and total apoptosis at 10.0 μM between 4MOD and TMZ (*P* < 0.001 4MOD vs. TMZ, Fig. 2g). Flow cytometry analysis demonstrated that the main effect of 4MOD on U87 cells was a decreased percentage of cells in G0/G1 phase and an increased percentage of cells in G2/M phase (Fig. 2d). Statistical analysis showed that the cells in the G0/G1 phase of the 4MOD untreated group decreased from 70.70% ± 9.32% to 44.33% ± 4.78% in the 5.0 μM 4MOD group (*P* < 0.01 vs. control); and 37.88% ± 5.97% in the 10.0 μM group (*P* < 0.0001 vs. control). G2/M phase cells of control and cells treated with 5.0 μM and 10.0 μM 4MOD accounted for 11.77% ± 1.57%, 35.76% ± 3.97% (*P* < 0.01 vs. control), and 43.27% ± 6.38% (*P* < 0.001 vs. control), respectively (Fig. 2e). TMZ did not affect cell

cycle at 10.0 μM, but blocked U87 cells at G2/M phase and S phase at 50.0 and 100.0 μM, respectively (Fig. 2f). Compared with 4MOD and TMZ, the difference of cellular G0/G1 phase (*P* < 0.001 4MOD vs. TMZ), and G2/M phase (*P* < 0.01 4MOD vs. TMZ) at 10.0 μM was statistically significant (Fig. 2h).

#### Transcriptome sequencing

To investigate possible mechanisms of 4MOD in inhibiting U87 astrogloma cells, we analyzed the transcription levels of associated mRNAs. Total RNAs were isolated from the control and 4MOD-treated groups and mRNA-sequencing was performed. A total of 362 differentially expressed genes (DEGs) were obtained with a fold change ≥ 2 and *q* < 0.01. Among these, 158 genes were found to be upregulated, and 204 genes were downregulated in the 4MOD-treated group compared with the control group (Fig. 3a, b). KEGG pathway enrichment analysis revealed the top 20 significantly enriched pathways that were directly associated with 4MOD. They were p53, p38, TNF, MAPK, FoxO, cell division, oocyte meiosis, cell cycle, cellular senescence, and ferroptosis (Fig. 3c). To determine the potential function of the DEGs, GO analyses including categories of biological process, cellular component (CC), and molecular function (MF) were performed. The results revealed that the DEGs were significantly enriched in GO005575 (cellular component, 100%), GO0005623 (cell, 94.81%), GO0044464 (cell part, 94.52%), GO0043227 (membrane-bounded organelle, 72.05%), GO0016020 (membrane, 46.11%), GO0043231 (intracellular membrane-bounded organelle, 69.45%), GO0043232

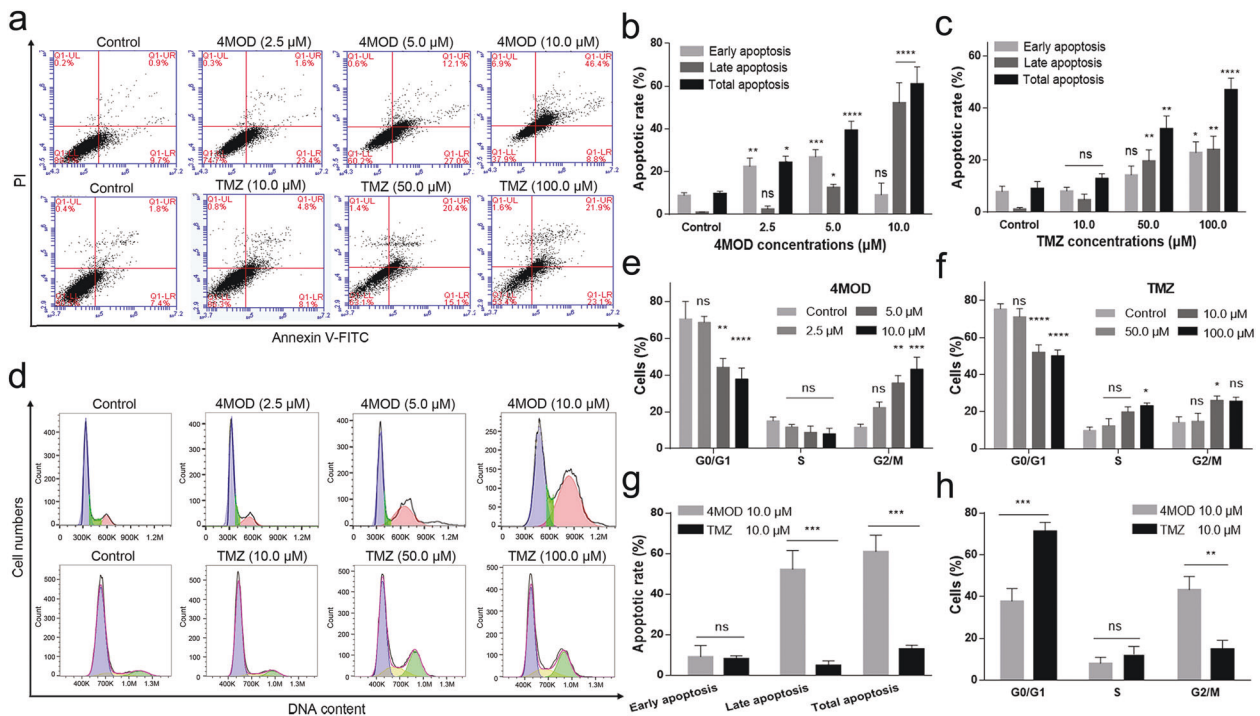


**Fig. 2** Effect of 4MOD and TMZ on apoptosis and the cell cycle of U87 astroglioma cells. **a** Cells treated with different concentrations of 4MOD and TMZ for 48 h. Cell apoptosis was detected by flow cytometry. The lower left represents normal cells, the lower right represents early apoptotic cells, the upper right represents late apoptotic cells, and the upper left represents dead or late apoptotic cells. **b, c** Analysis of the altered rates of early apoptosis, late apoptosis, and total apoptosis after 4MOD and TMZ treatment. **d** Cells treated with different concentrations of 4MOD and TMZ for 48 h, stained with propidium iodide (PI), and subjected to flow cytometry analysis to determine their distribution in each phase of the cell cycle. Different colors from left to right represent G0/G1, S, and G2/M phase cells, respectively. **e, f** Altered cell cycle distribution of U87 cells after 48 h treatment with different 4MOD and TMZ concentrations. Results are expressed as means  $\pm$  SEM,  $n = 3$ , \* $P < 0.05$ , \*\* $P < 0.01$ , \*\*\* $P < 0.001$ , \*\*\*\* $P < 0.0001$  vs. the control group. **g** Comparison of apoptosis rates between 4MOD and TMZ, \*\*\* $P < 0.001$ , 4MOD vs. TMZ. **h** Comparison of cell cycle between 4MOD and TMZ, \*\* $P < 0.01$ , \*\*\* $P < 0.001$ , 4MOD vs. TMZ.

(intracellular non-membrane-bounded organelle, 40.06%), GO0044424 (intracellular part, 84.15%), GO0044422 (organelle part, 84.15%), GO0044429 (intracellular organelle, 75.5%), GO0044446 (intracellular organelle part, 56.48%), GO0044430 and GO0005634 (nucleus, 51.59%), GO0044428 (nuclear part, 40.06%), and GO0005737 (cytoplasm, 68.3%) (Fig. 3d). These results suggest that 4MOD interferes with cell mitosis, blocks cell cycling, destroys the integrity of cell membrane and cell structure, and leads to cell apoptosis, which may underlie 4MOD-induced tumor cell death.

Quantitative real-time PCR analyses of protein–protein interaction after 4MOD treatment

STRING and Cytoscape software were used to extract a protein–protein interaction network of the DEGs to evaluate potential interactions of the hub genes following 5.0  $\mu$ M 4MOD treatment for 12 h. A total of 17 genes were identified from the protein–protein interaction network, including RRM2, MCM7, BUB1B, CCNA2, CCNB1, CDC20, CCNB2, CDK1, MAP2K6, PLK1, ATF4, SESN2, HSPB1, IL-1A, IL-6, BCL-2, and BUB1 (Fig. 4a). These genes mainly concentrated in the cell cycle, apoptosis and tumor suppression-related signaling pathways.

Further, the gene expression levels, using the  $2^{-\Delta\Delta CT}$  method and normalization to GAPDH as a reference, were determined. The 17 DEGs between 4MOD-treated (5.0  $\mu$ M treatment for 12 h) and -untreated groups were selected and verified using RT-qPCR. The results showed that four hub genes were found to be over-expressed (Fig. 4b), and 13 genes were under expressed in the 4MOD treatment group (Fig. 4c). The results were consistent with the sequencing data.

4MOD inhibits U87 astroglioma growth in the BALB/c-nu mouse model

Data presented thus far demonstrate that 4MOD remarkably inhibits U87 cell growth in an in vitro cell line. We used transplanted U87 cells into nude mice (BALB/c-nu mice) and then examined the increase in tumor volume with and without 4MOD treatment. Beginning 20 days after tumor cell implantation, 4MOD was administered at a dose of 10 or 30 mg/kg, once per 3 days for 27 days. Tumor volume was measured every 3 days using a small animal ultrasonic 2D and 3D imaging platform. In 2D images, each 1.0 mm of tumor image was measured, and the tumor boundary was represented by blue lines (Fig. 5a). According to the cross-section measurement data, the 3D shape of the tumor was fitted by VsiApp software (Fig. 5b). In this way, the tumor volumes were obtained. As shown in Fig. 5c, the tumor volume was smaller in 4MOD group ( $n = 6$ , 10 mg/kg group,  $85.67 \pm 12.21 \text{ mm}^3$ ) at day 21, as compared with the control group ( $n = 6$ ,  $127.49 \pm 12.02 \text{ mm}^3$ ,  $P < 0.001$ ). Tumor volume was decreased significantly after 9 days of 4MOD treatment in the 30 mg/kg group ( $59.04 \pm 3.33 \text{ mm}^3$ ,  $P < 0.01$  vs. control group,  $n = 6$ ). On the last day (day 27), tumor tissues were removed and weighed (Fig. 5d), tumor weights were  $0.141 \pm 0.026 \text{ g}$  in untreated control group ( $n = 6$ ),  $0.075 \pm 0.007 \text{ g}$  in 10 mg/kg treated group, ( $n = 6$ ,  $P < 0.05$  vs. control), and  $0.043 \pm 0.011 \text{ g}$  in 30 mg/kg group ( $P < 0.01$  vs. control, Fig. 5e).

We also applied RT-qPCR to verify the expression levels of G2 phase-related genes, such as the p53 signaling pathway (CCNB1, CCNB2, CDK1) and apoptosis (Bcl-2, Bax)-related genes, for tumor tissue. The expressions of CCNB1, CCNB2, and CDK1 were significantly downregulated in the low dose 10 mg/kg group. The expressions of p53 and Bcl-2 were also significantly decreased

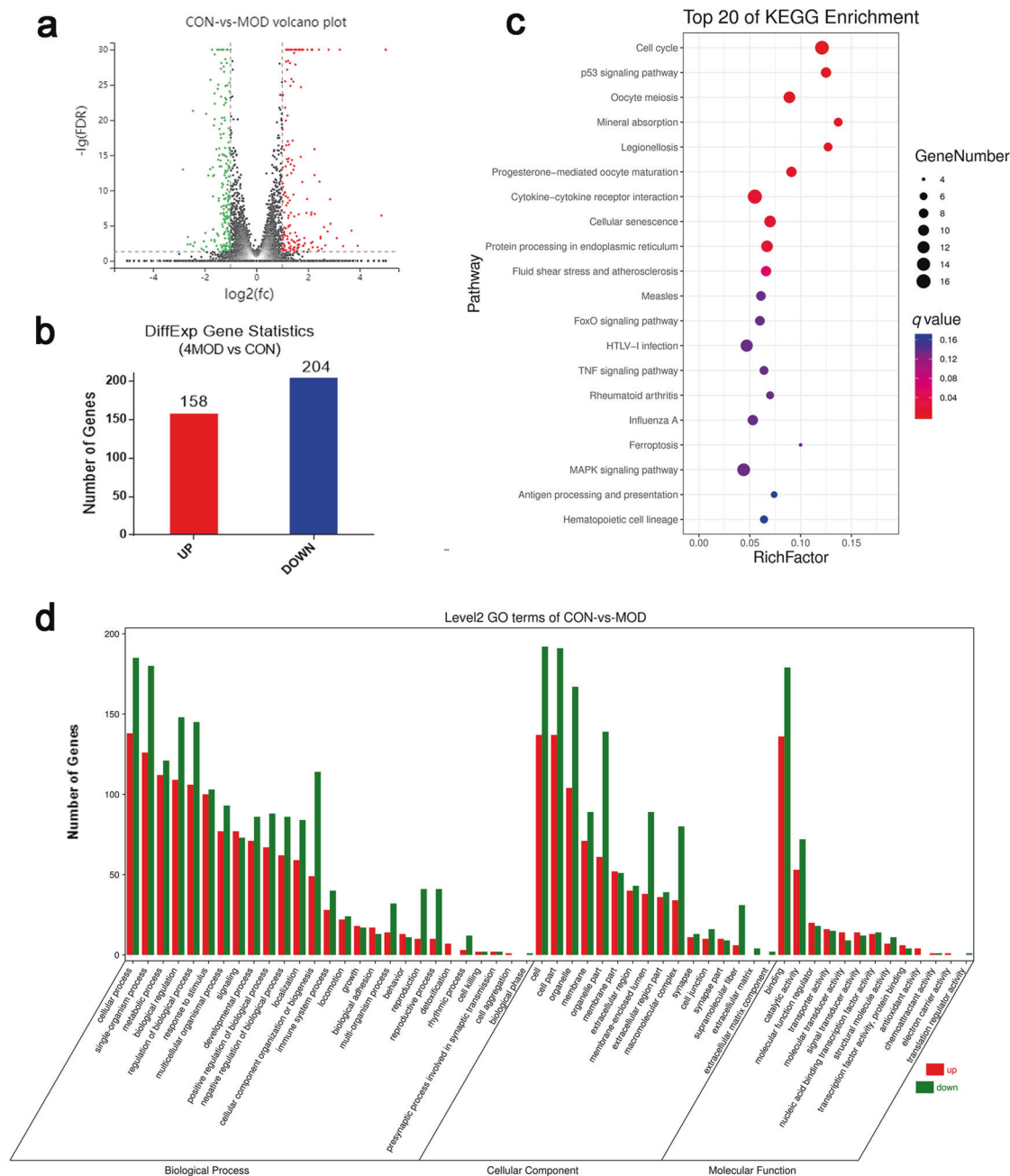


**Fig. 3** GO/KEGG pathway enrichment analysis of DEGs. **a** Volcano plots analyzing differential expressions of mRNA in U87 cells. Green dots represent downregulated genes, and red dots represent upregulated genes. **b** Histogram showing the differentially expressed mRNA in U87 cells, 158 genes were upregulated, and 204 genes were downregulated. **c** Differentially expressed mRNA on the top 20 pathways identified by KEGG analysis. Bubble size represents the number of DEGs enriched in a signaling pathway; the bubble color represents the *q* value. **d** GO enrichment analysis of the significantly upregulated and downregulated genes. Red columns are the numbers of up-regulated DEGs related to this function, and green columns are the numbers of down-regulated DEGs; DEGs were chosen by a fold change  $\geq 2$  and  $q < 0.01$ .

at high doses (30 mg/kg group). The results are consistent with our in vitro experiments (Fig. 5f).

Further, we examined the effects of TMZ in this in vivo U87 tumor model. The tumor volume was significantly smaller in the treatment group of TMZ (30 mg/kg group,  $95.33 \pm 7.99 \text{ mm}^3$ ,  $n = 3$ ) at day 9, as compared with the control group ( $138.89 \pm 11.22 \text{ mm}^3$ ,  $P > 0.05$ ) (Fig. S5a). Tumor weights were  $0.135 \pm 0.024 \text{ g}$  (control group),  $0.081 \pm 0.011 \text{ g}$  (30 mg/kg group,  $P > 0.05$  vs. control) (Fig. S5b). Comparison between 4MOD and TMZ, after 9 following initiation of treatment, the difference in tumor size reduction (4MOD reduced  $74.8\% \pm 4.3\%$  vs. TMZ reduced  $1.9\% \pm 0.2\%$ ,  $P < 0.0001$ ) and the

difference in tumor weights (4MOD reduced  $69.5\% \pm 6.8\%$  vs. TMZ  $41.2\% \pm 2.5\%$ ,  $P < 0.05$ ) were statistically significant.

Toxicity observation for 4MOD in vivo and in BV2 microglia cells H&E staining showed only a few enlarged nuclei (Liver, black arrows). Kidney displayed no significant differences between control and 4MOD treatment groups (Fig. S1a, b). In addition, we monitored the weight among the control group and different 4MOD treatment groups. No significant differences were observed among them (Fig. S1c). BV2 is a normal microglia cell line. 4MOD-treated BV2 cells exhibited no obvious morphological changes

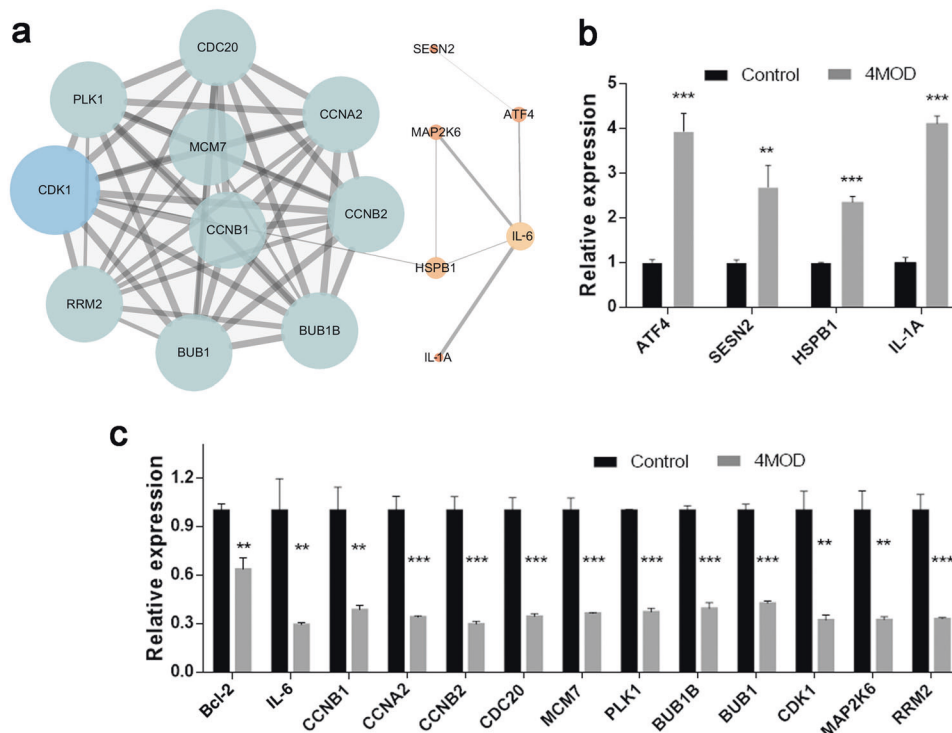


**Fig. 4 Validation of DEGs by qRT-PCR.** **a** Protein–protein interaction network of the differentially expressed genes after 4MOD treatment. The color of the circle represents the action type of the corresponding interaction relationship and is a qualitative attribute; the size of the circle represents quantitative attributes; the line represents the functional correlation of the prediction, and the thickness represents the degree of confidence of the interaction. **b** Relative expression of DEGs as verified by qRT-PCR. The results indicated that the relative expressions of ATF4, SESN2, HSPB1, and IL-1A in the 4MOD group were higher than control group. **c** The expression of Bcl-2, IL-6, CCNB1, CCNA2, CCNB2, CDC20, MCM7, PLK1, BUB1B, BUB1, CDK1, MAPSK6, and RRM2 in the 4MOD group were lower than control group. Results are expressed as the means  $\pm$  SEM,  $n = 3$ ,  $**P < 0.01$ ;  $***P < 0.001$  vs. the control group.

compared with the untreated control cells (Fig. S4a). Cell viability was determined using the CCK8 assay, which demonstrated that 4MOD promoted cell proliferation at low concentrations and showed toxic effects at high concentration (Fig. S4b). 4MOD showed significant differences in the inhibitory concentrations for tumor cells vs. microglia cells, which was helpful in controlling the dose (Fig. S4c).

## DISCUSSION

In this study, 4MOD was shown to inhibit U87 astroglioma cell proliferation and induce cell apoptosis. Inhibition of tumor cell proliferation and induction of the apoptosis are important in tumor progression [12, 13], and several antitumor drugs work by inducing apoptosis in tumor cells [14]. Our results also show that 4MOD increases early and late apoptosis. Cell cycle changes are reported to be important markers of apoptosis [15], and they are closely related to tumor development [16]. Stupp's team has reported that regulating cell cycle through TTFIELDS can induce apoptosis and significantly improve patient survival [17]. They also demonstrated that TMZ intervention can significantly improve patient survival through multi-center clinical studies [3]. It will play an important guiding role in developing 4MOD as a new candidate for treatment of brain astroglioma. The present study found that 4MOD altered the U87 cell cycle by decreasing the percentage of cells in G0/G1 phase and increasing the percentage of cells in the G2/M phase. TMZ decreased the percentage of cells in the G0/G1 phase and increased the percentage of cells in the G2/M and S phase. But the concentration difference between them is large. In addition, the  $IC_{50}$  values of 4MOD at 24, 48, and 72 h were tenfold lower than TMZ. Usually, anti-tumor drugs show side effects at higher concentration. Thus, our results suggest that

use of 4MOD could be of interest in reducing the toxic and side effects of chemotherapy drugs, as well as enhancing efficacy.

Transcriptome analysis is an effective method used to investigate anticancer effects and mechanisms [18]. In this study, we sequenced the transcriptome of cells (4MOD treated group and control group) and verified the changes in gene expression with qPCR. In addition, functional analyses of DEGs were explored using KEGG and GO in STRING. We observed a downregulation of functional clusters related to the cell cycle, including RRM2, MCM7, BUB1B, CCNA2, CCNB1, CDC20, CCNB2, CDK1, PLK1, and BUB1. These genes play critical roles in regulating DNA replication and repair, which may indirectly influence the cell cycle [19, 20]. Cyclins are positive regulatory units for CDKs whose activity is negatively regulated by a variety of CDKs inhibitors. These inhibitors play a key role in the transition from G2 to M phase of the cell cycle [21]. Among them, the protein encoded by CCNB1 is a regulatory protein involved in mitosis and it is important in the regulation of the G2/M transition phase of the cell cycle [22, 23]. Furthermore, it has also been pointed out that downregulation of CCNB1 mRNA levels and protein reduces cell proliferation [24]. CDK activity increases or decreases as the cell cycle progresses. Among the CDKs, the CDK1/cyclin B complex is known to control G2/M transition, while the CDK2/cyclin E1/A complex regulates G1/S and S/G2 transitions [25]. CDC20, BUB1, and BUB1B are the targets of the spindle assembly checkpoint and they ensure faithful segregation of chromosomes [26, 27]. Downregulation of BUB1 and BUB1B expression accelerates the progression from G1 to S phase and reduces G1 accumulation. Therefore, this study reveals how 4MOD arrested the G2/M phase of the cell cycle and induced cell apoptosis.

Many compounds have anti-tumor effects in vitro, but not in vivo because there may be many influencing factors in the

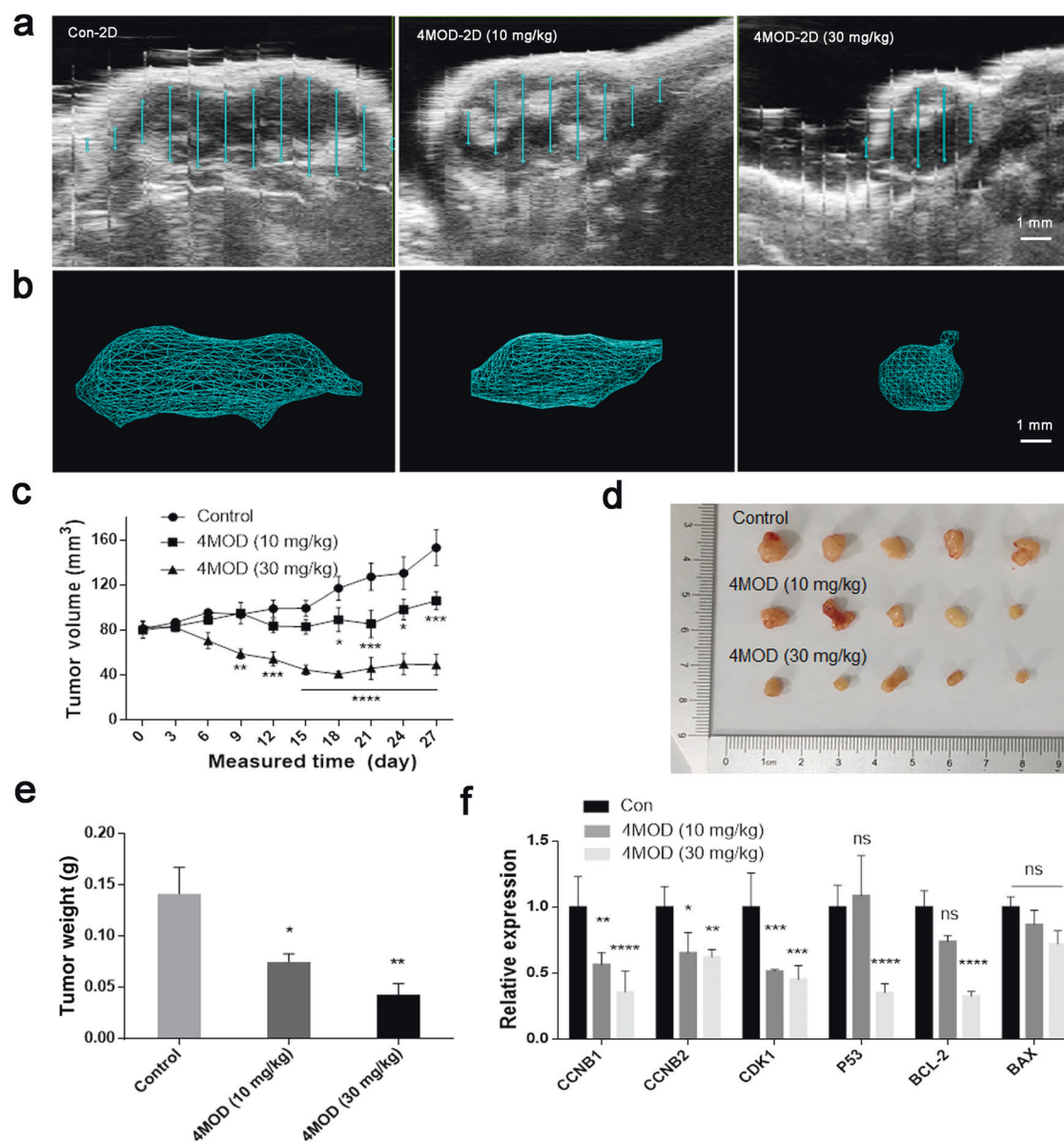


**Fig. 5 4MOD inhibits U87 tumor growth in BALB/c-nu mice.** **a** Ultrasound images (2D images) of the cross-section view of tumors collected using a small animal ultrasonic 3D imaging platform. The blue lines represent measurements of the tumor boundary at intervals of 1.0 mm on this section. **b** 3D reconstruction of tumors and the tumor volume determined using 3D fitting. Tumor volume was also calculated by this procedure. **c** Drug administration time and tumor volume change curves. **d** Tumor tissue sizes after 4MOD treatment. **e** Tumor weight plot. Results are expressed as the means  $\pm$  SEM,  $n = 6$ ,  $*P < 0.05$ ,  $**P < 0.01$ ,  $***P < 0.001$ ,  $****P < 0.0001$  vs. the control group. **f** Expression of CCNB1, CCNB2, CDK1, p53, BCL-2, and BAX in tumors of the 4MOD groups and control group. Results are expressed as the means  $\pm$  SEM,  $n = 3$ ,  $*P < 0.05$ ;  $**P < 0.01$ ;  $***P < 0.001$ ,  $****P < 0.0001$  vs. the control group.

in vivo environment. In this study, based on our in vitro findings, the in vivo antitumor efficacy of 4MOD was evaluated in BALB/c-nu tumor-bearing mice. 4MOD was found to reduce tumor growth. This inhibition of tumor growth was positively correlated with dose and administration time. These findings confirm the antitumor properties of 4MOD against astrogloma and are also consistent with the in vitro properties.

4MOD is one of the flavonoids found in *D. sissoo* Roxb. Flavonoids have been reported to have antioxidant and anti-tumor activities [28–30]. The anti-tumor effect of flavonoids has been associated with the induction of tumor cell apoptosis, inhibition of the cell cycle, tumor neovascularization, cyclooxygenase 2, and regulation of immunosuppressive telomerase activity [31, 32]. The latest research also directly shows 4MOD has anti-osteosarcoma effect [7]. The molecular weight of 4MOD is

254.28 and it is mainly concentrated in low-polarity sites such as chloroform, our study also demonstrates that it can cross the BBB. So, it may have a therapeutic effect on brain-related diseases. Astrogloma is a major tumor that occurs in the brain.

This study demonstrates 4MOD exerts antitumor effects on U87 astrogloma cells both in vivo and in vitro. To the best of our knowledge, this is the first study to evaluate the antitumor action and apoptotic potential of 4MOD on astrogloma cells. Besides, previous studies have reported that 4MOD possesses anti-inflammatory and cell-protective effects in hippocampal BV2 microglia cells in mice and primary microglia in rats [8]. We also found that 4MOD has proliferative effects on BV2 cells at low concentrations ( $<10.0 \mu\text{M}$ ) but was toxic to cells at high concentrations ( $>10.0 \mu\text{M}$ ) (Fig. S4). In order to explore the toxicity of 4MOD, we verified the liver and kidney tissue side effects in



mouse models. HE staining showed no significant difference between control and 4MOD (30 mg/kg)-treated group. In addition, we monitored the weight among the control group and 4MOD treatment groups treated with different doses of 4MOD. This also showed no significant difference among them (Fig. S1). All the studies have suggested that 4MOD may be less toxic to normal cells, though this is subject to further toxicological investigations. This study provides new insides into the pharmacological effects of 4MOD and its potential as a new treatment for astrogloma.

## ACKNOWLEDGEMENTS

We are grateful to Professor Kang-sheng Li, Yi Guan, Dr. Chun-yan Li, Dr. Tian Li and Mr. Ge-jun Li for their technical assistance and experimental material support. This work was supported by the Research Foundation of Hunan Administration of Traditional Chinese Medicine (No. 2019101); Natural Science Foundation of Hunan province (No. 2019JJ50631); Research Foundation of Guangdong Administration of Traditional Chinese Medicine (No. 20202090).

## AUTHOR CONTRIBUTIONS

JW, RL, XYJ designed the research and wrote the article; CQX, JXS, DLC, MJL directed the experiment and data analysis; CQX, RL, RNH, ZHL performed the vitro experiments and analyzed the data; RL, QYR, CHL, RTZ did the in vivo experiments and analyzed the data.

## ADDITIONAL INFORMATION

The online version of this article (<https://doi.org/10.1038/s41401-020-00560-w>) contains supplementary material, which is available to authorized users.

**Conflict of interest:** The authors declare that they have no conflict of interest.

**Ethical approval:** All experimental procedures in the current study were approved by Shan tou University Animal Care Committee (approval number: SUMC2019-173).

## REFERENCES

1. Bray F, Ferlay J, Soerjomataram I, Siegel RL, Torre LA, Jemal A. Global cancer statistics 2018: GLOBOCAN estimates of incidence and mortality worldwide for 36 cancers in 185 countries. *CA Cancer J Clin.* 2018;68:394–424.
2. Gao J, Wang Z, Liu H, Wang L, Huang G. Liposome encapsulated of temozolomide for the treatment of glioma tumor: preparation, characterization and evaluation. *Drug Discov Ther.* 2015;9:205–12.
3. Stupp R, Mason WP, van den Bent MJ, Weller M, Fisher B, Taphoorn MJ, et al. Radiotherapy plus concomitant and adjuvant temozolomide for glioblastoma. *N Engl J Med.* 2005;352:987–96.
4. Yu ZY, Xie GF, Zhou GT, Cheng Y, Zhang GT, Yao GM, et al. NVP-BEZ235, a novel dual PI3K-mTOR inhibitor displays anti-glioma activity and reduces chemoresistance to temozolomide in human glioma cells. *Cancer Lett.* 2015;367:58–68.
5. National Pharmacopoeia Committee. *Pharmacopoeia of the People's Republic of China (part I)*. Beijing: China Medical Science and Technology Press; 2015. p. 229–30.
6. Hirano T, Abe K, Gotoh M, Oka K. Citrus flavone tangeretin inhibits leukaemic HL-60 cell growth partially through induction of apoptosis with less cytotoxicity on normal lymphocytes. *Br J Cancer.* 1995;72:1380–8.
7. Park KR, Yun HM, Quang TH, Oh H, Lee DS, Auh QS, et al. 4-Methoxydalbergione suppresses growth and induces apoptosis in human osteosarcoma cells in vitro and in vivo xenograft model through down-regulation of the JAK2/STAT3 pathway. *Oncotarget.* 2016;7:6960–71.
8. Kim DC, Lee DS, Ko W, Kim KW, Kim HJ, Yoon CS, et al. Heme Oxygenase-1-inducing activity of 4-methoxydalbergione and 4-hydroxy-4-methoxydalbergione from *Dalbergia odorifera* and their anti-inflammatory and cytoprotective effects in murine hippocampal and BV2 microglial cell line and primary rat microglial cells. *Neurotox Res.* 2018;33:337–52.
9. Chan SC, Chang YS, Wang JP, Chen SC, Kuo SC. Three new flavonoids and anti-allergic, anti-inflammatory constituents from the heartwood of *Dalbergia odorifera*. *Plant Med.* 1998;64:153–8.
10. Li R, Xu CQ, Qi LK, Li J, Li CH, Cai C, et al. Separation and structures identification of chemical components in *Dalbergia sissoo* Roxb. *J Guangdong Pharm Univ.* 2019;35:9–15.
11. Li R, Lin L, Qi LK, Du HF, Li J, Cai C, et al. Quantitative determination of dalbergin and other two compounds in *Dalbergia sissoo* Roxb. by HPLC. *J Guangdong Pharm Coll.* 2016;32:51–4.
12. Cobbs CS. Cytomegalovirus and brain tumor: epidemiology, biology and therapeutic aspects. *Curr Opin Oncol.* 2013;25:682–8.
13. Bartuzi P, Hofker MH, van de Sluis B. Tuning NF- $\kappa$ B activity: a touch of COMMD proteins. *Biochim Biophys Acta.* 2013;1832:2315–21.
14. Jin XH, Shi YI. Isobavachalcone induces the apoptosis of gastric cancer cells via inhibition of the Akt and Erk pathways. *Exp Ther Med.* 2016;11:403–8.
15. Pietenpol JA, Stewart ZA. Cell cycle checkpoint signaling cell cycle arrest versus apoptosis. *Toxicology.* 2002;181-182:475–81.
16. Mills C, Kolb EA, Sampson VB. Recent advances of cell-cycle inhibitor therapies for pediatric cancer. *Cancer Res.* 2017;77:6489–98.
17. Stupp R, Taillibert S, Kanner A, Read W, Steinberg DM, Lhermitte B, et al. Effect of tumor-treating fields plus maintenance temozolomide vs maintenance temozolomide alone on survival in patients with glioblastoma. *JAMA.* 2017;318:2306–16.
18. Tang F, Barbacioru C, Wang Y, Nordman E, Lee C, Xu N, et al. mRNA-Seq whole-transcriptome analysis of a single cell. *Nat Methods.* 2009;6:377–82.
19. Huang K, Sun J, Yang C, Wang Y, Zhou B, Kang C, et al. HOTAIR upregulates an 18-gene cell cycle-related mRNA network in glioma. *Int J Oncol.* 2017;4:1271–8.
20. Kapanidou M, Curtis NL, Bolanos-Garcia VM. Cdc20: At the crossroads between chromosome segregation and mitotic exit. *Trends Biochem Sci.* 2017;42:193–205.
21. Lu MC, Yang SH, Hwang SL, Lu YJ, Lin YH, Wang SR, et al. Induction of G2/M phase arrest by squamocin in chronic myeloid leukemia (K562) cells. *Life Sci.* 2006;78:2378–83.
22. Allan K, Jordan RC, Ang LC, Taylor M, Young B. Overexpression of cyclin A and cyclin B1 proteins in astrocytomas. *Arch Pathol Lab Med.* 2000;124:216–20.
23. Haas DM, Lai D, Sharma S, Then J, Kho A, Flockhart DA, et al. Steroid pathway genes and neonatal respiratory distress after betamethasone use in anticipated preterm birth. *Reprod Sci.* 2016;23:680–6.
24. Mussnich P, Raverot G, Jaffrain-Rea ML, Frassetto F, Wierinckx A, Trouillas J, et al. Downregulation of miR-410 targeting the cyclin B1 gene plays a role in pituitary gonadotroph tumors. *Cell Cycle.* 2015;14:2590–7.
25. Yoon IS, Chung JH, Hahn SH, Park MJ, Lee YR, Ko SJ, et al. Ribosomal protein S3 is phosphorylated by Cdk1/cdc2 during G2/M phase. *BMB Rep.* 2011;44:529–34.
26. Raaijmakers JA, van Heesbeen RG, Blomen VA, Janssen LM, van Diemen F, Brummelkamp TR, et al. BUB1 is essential for the viability of human cells in which the spindle assembly checkpoint is compromised. *Cell Rep.* 2018;22:1424–38.
27. Kops GJ, Foltz DR, Cleveland DW. Lethality to human cancer cells through massive chromosome loss by inhibition of the mitotic checkpoint. *Proc Natl Acad Sci U S A.* 2004;101:8699–704.
28. Garcia-Lafuente A, Guillaumon E, Villares A, Rostagno MA, Martinez JA. Flavonoids as anti-inflammatory agents: implications in cancer and cardiovascular disease. *Inflamm Res.* 2009;58:537–52.
29. Zain WN, Rahmat A, Othman F, Yap TY. Antiproliferative properties of Clausine-B against cancer cell lines. *Malays J Med Sci.* 2009;16:31–6.
30. Lai CS, Tsai ML, Cheng AC, Li S, Lo CY, Wang Y, et al. Chemoprevention of colonic tumorigenesis by dietary hydroxylated polymethoxyflavones in azoxymethane-treated mice. *Mol Nutr Food Res.* 2010;55:278–90.
31. Liao CY, Lee CC, Tsai CC, Hsueh CW, Wang CC, Chen IH, et al. Novel investigations of flavonoids as chemopreventive agents for hepatocellular carcinoma. *Biomed Res Int.* 2015;2015:1–26.
32. Yang N, Jia XB, Zhang ZH, Sun E, Yan HM. Advances in antitumor activity and mechanism of flavonoids compounds. *Chin J Tradit Chin Med.* 2015;40:373–81.